

## Laser scattering measurements of thermal ion-acoustic fluctuations in collisionally dominated plasmas

Andrew N. Mostovych\* and Alan W. DeSilva

Laboratory for Plasma and Fusion Energy Studies, University of Maryland, College Park, Maryland 20742

(Received 23 August 1985)

The thermal ion-acoustic fluctuation spectrum of a high-density, low-temperature ( $10^{17} \text{ cm}^{-3}$ , 2 eV) collisional plasma was measured using  $\text{CO}_2$ -laser scattering. The measured spectra differed substantially from spectra observed in collisionless plasmas. Fluctuations at the ion-acoustic frequency were strongly enhanced and the width of the resonance was significantly narrowed in comparison to the collisionless case. Comparison to the predictions of various collisional theories shows the Bhatnagar-Gross-Krook theory to be the most successful in describing the data.

### I. INTRODUCTION

The fluctuation behavior of equilibrium plasmas is determined by two basic processes: the discrete collisions between particles and the collective interactions of particles with the average fields of the system. The relative importance of these interactions is characterized by the plasma parameter  $g = 1/n\lambda_D^3$ , which is the inverse of the number of particles in a Debye cube and which measures the ratio of the mean interparticle potential energy to the mean plasma kinetic energy. If the plasma parameter is small, as is the case for most laboratory and astrophysical plasmas, many particles participate in setting up the collective fields around any individual particle and thus the effects of two-particle correlations (i.e., collisions) are not important. As a consequence, most of the kinetic theory that has been developed to model the fluctuation behavior of plasmas depends on expansions in  $g$  and does not specifically consider collisional effects. There are, however, some plasmas, such as the ones found in the interior of stars, in inertial confinement fusion experiments, and in dense, low-temperature arcs, that are strongly influenced by collisions and for which  $g$  is no longer small. As a result, the standard collisionless theories are inadequate in treating such plasmas. Efforts to generalize the theory have been made by several authors;<sup>1-6</sup> however, these theories differ in their predictions and current experimental data<sup>7-9</sup> are insufficiently precise to test their validity.

In this paper we compare the various theoretical predictions and we present laser scattering measurements of thermal ion-acoustic fluctuations from dense, low-temperature ( $n = 10^{17} \text{ cm}^{-3}$ ,  $T_e = 2 \text{ eV}$ ), i.e., collisional, helium, and argon plasmas which are used to test the theoretical predictions in the collisional regime. To insure that comparison to theory can be made without resorting to parameter fitting schemes, the plasmas are also fully diagnosed by independent spectroscopic, interferometric, and probe measurements.

Ion-acoustic fluctuations were selected because of their high sensitivity to the effects of collisions, given their relatively low frequency. In particular, the degree to which the scattering spectra can be expected to be altered by the

presence of collisions is determined by the ratio ( $v_{ii}/kC_s$ ) of the ion-ion collision frequency to the ion-acoustic frequency  $kC_s$  [where  $k = 4\pi/\lambda_0 \sin(\theta/2)$  is the fluctuation wave number and  $C_s = (\gamma kT/m)^{1/2}$  is the ion-acoustic velocity,  $\theta$  represents scattering angle, and  $m$  is ion mass]. If  $v_{ii}/kC_s \geq 1$ , collisional effects are important and for given plasma conditions they can be maximized by a choice of small wave numbers. In this work collisional effects were maximized by the use of a long-wavelength ( $\lambda_0 = 10.6 \mu\text{m}$ )  $\text{CO}_2$  laser and small scattering angles ( $4^\circ - 9^\circ$ ). This choice of scattering parameters was, in fact, ideally suited to test the validity of the various theories, since in this parameter regime the predicted ion-acoustic fluctuation spectra vary substantially from theory to theory, as is demonstrated by the calculations presented in Fig. 1.

This paper is organized in the following way. Section II provides a review of laser scattering theory. A discussion of the various theoretical models which are applicable to the study of collisional plasmas is presented in Sec. III, the validity of the theories is examined, and their pre-

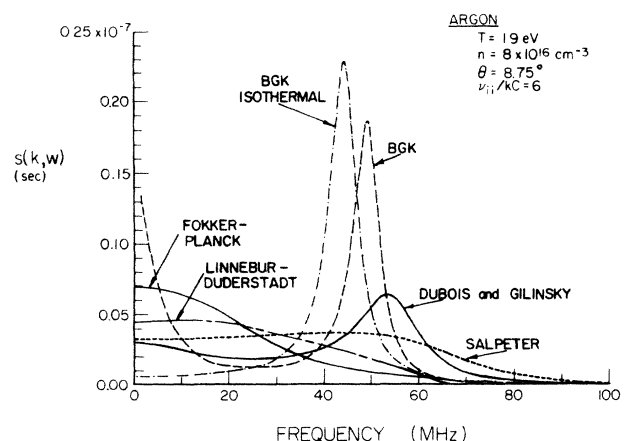


FIG. 1. Ion-acoustic spectra for a collisional argon plasma as calculated from the various collisional theories (Refs. 1-5) and compared to a collisionless calculation [Salpeter (Ref. 14)].

dictions of the ion-acoustic fluctuation spectra are given. In Sec. IV we describe the experiment. This includes the plasma source, its properties, and the laser scattering set-up. The scattering results are presented in Sec. V, while the interpretations and conclusions are found in Secs. VI and VII, respectively.

## II. SCATTERING THEORY

### A. Review of scattering theory

The power spectrum of light which is scattered by a plasma automatically contains the frequency and wavelength spectrum of density fluctuations that are endemic to the plasma. The relationship between the spectrum of scattered light and the plasma density fluctuations is given by<sup>10</sup>

$$S(\mathbf{k}, \omega) = \lim_{T \rightarrow \infty} \lim_{V \rightarrow \infty} \left[ \frac{1}{TV} \int d\mathbf{r} \int d\mathbf{r}' \int dt \int dt' \langle n(\mathbf{r}, t) n^*(\mathbf{r}', t') \rangle e^{-i\omega(t-t')} e^{i\mathbf{k} \cdot (\mathbf{r}-\mathbf{r}')} \right]. \quad (3)$$

For a stationary process,  $\langle n(\mathbf{r}, t) n^*(\mathbf{r}', t') \rangle$  is only a function of  $\tau = t - t'$  and  $\mathbf{R} = \mathbf{r} - \mathbf{r}'$ ; thus, Eq. (3) can be integrated to yield

$$S(\mathbf{k}, \omega) = \frac{2}{n} \int d\mathbf{R} \int d\tau \langle n(\mathbf{O}, 0) n^*(\mathbf{R}, \tau) \rangle e^{-i\omega\tau} e^{i\mathbf{k} \cdot \mathbf{R}} \quad (4)$$

from which one can readily identify  $\langle n(\mathbf{O}, 0) n^*(\mathbf{R}, \tau) \rangle$  as the velocity-independent pair correlation function. As a result, scattering experiments, in addition to measuring the density fluctuation spectrum of the plasma, also obtain valuable information about pair correlations in the plasma.

$$\frac{\partial f_\alpha}{\partial t} + \mathbf{v} \cdot \frac{\partial f_\alpha}{\partial \mathbf{r}} + \frac{q_\alpha}{m_\alpha} \mathbf{E} \cdot \frac{\partial f_\alpha}{\partial \mathbf{v}} = \frac{\partial}{\partial \mathbf{v}} \cdot \sum_\beta \frac{\bar{n}_\beta}{\bar{n}_\alpha} \int d\mathbf{k} \frac{\mathbf{k}}{m_\alpha} \omega_{p\alpha}^2 q_{\beta} \int \frac{\delta(\mathbf{k} \cdot \mathbf{v} - \mathbf{k} \cdot \mathbf{v}')}{|\epsilon(\mathbf{k}, \omega - i\mathbf{k} \cdot \mathbf{v})|^2} \left[ \frac{1}{m_\alpha} \frac{\partial}{\partial \mathbf{v}} - \frac{1}{m_\beta} \frac{\partial}{\partial \mathbf{v}'} \right] f_\alpha(\mathbf{v}, t) f_\alpha(\mathbf{v}', t) d\mathbf{v}' \quad (5)$$

and a spectral density function given by

$$S(\mathbf{k}, \omega) = 2\pi \left[ \frac{|G_i(\mathbf{k}, \omega) + 1|^2}{|\epsilon(\mathbf{k}, \omega)|^2} \int f_e(\mathbf{v}) \delta(\omega - \mathbf{k} \cdot \mathbf{v}) + \frac{|G_e(\mathbf{k}, \omega)|^2}{|\epsilon(\mathbf{k}, \omega)|^2} \int f_i(\mathbf{v}) \delta(\omega - \mathbf{k} \cdot \mathbf{v}) d\mathbf{v} \right] \quad (6)$$

with

$$\epsilon(\mathbf{k}, \omega) = 1 + G_i(\mathbf{k}, \omega) + G_e(\mathbf{k}, \omega)$$

and

$$G_\alpha(\mathbf{k}, \omega) = \frac{v_\alpha^2}{\lambda_D^2 k^2} \int_L d\mathbf{v} \frac{1}{\omega - \mathbf{k} \cdot \mathbf{v}} \mathbf{k} \cdot \frac{\partial f_\alpha(\mathbf{v})}{\partial \mathbf{v}},$$

where  $L$  refers to a Landau contour,  $v_\alpha$  is the thermal velocity, and  $f(v)$  is the single-particle distribution func-

$$\left\langle \frac{d^2 P}{d\Omega d\omega} \right\rangle = \frac{P_0}{2\pi} n_e L_v r_0^2 |\hat{\mathbf{s}} \times (\hat{\mathbf{s}} \times \hat{\mathbf{E}})|^2 S(\mathbf{k}, \omega), \quad (1)$$

where  $\mathbf{k} = \mathbf{k}_s - \mathbf{k}_i$  and  $\omega = \omega_s - \omega_i$  are the respective fluctuation wave number and frequency and where  $P_0$  is the incident laser power,  $n_e$  the electron density,  $L_v$  the length of the scattering volume,  $r_0$  the classical electron radius, and  $\hat{\mathbf{s}}$  and  $\hat{\mathbf{e}}$  the unit vectors in the direction of the scattered light and incident electric field, respectively.

The spectral density function  $S(\mathbf{k}, \omega)$  is defined by

$$S(\mathbf{k}, \omega) = \lim_{T \rightarrow \infty} \lim_{V \rightarrow \infty} \left[ \frac{2}{TV} \frac{\langle n(\mathbf{k}, \omega) n^*(\mathbf{k}, \omega) \rangle}{n} \right] \quad (2)$$

and represents the density fluctuations of the plasma. The spectral density function  $S(\mathbf{k}, \omega)$  can also be written in terms of its Fourier transforms in the following way:

### B. Evaluation of the spectral density function from BBGKY theory

The standard method by which the spectral density function is obtained is by calculating the pair correlation function from a Bogolyubov-Born-Green-Kirkwood-Yvon<sup>11</sup> (BBGKY) hierarchy of Klimontovich<sup>12</sup> equations. This hierarchy of equations corresponds to expansions in the plasma parameter  $g = 1/n\lambda_D^3$ , which must be small to allow for truncation of the hierarchy.

To include discrete particle correlations, the BBGKY hierarchy must be solved to at least the first order in the plasma parameter. Such a solution produces the Balescu-Lenard equation for the single-particle distribution function<sup>13</sup>

tion governed by the Balescu-Lenard equation.

The form of the electron spectral density function naturally breaks up into two separate terms: the first of these corresponds to collective density fluctuations of the electrons, while the second term corresponds to fluctuations in the electron density that are due to fluctuations in the ion density and are coupled to the electrons through collective electric fields. Both terms have the plasma dielectric function  $\epsilon(\mathbf{k}, \omega)$  in their denominator; as a result, the magnitude of these terms is only appreciable at the frequencies corresponding to the normal modes of the plasma [i.e.,  $\epsilon(\mathbf{k}, \omega) = 0$ ]. For electrons, there should be a resonance at a frequency corresponding to Langmuir waves  $\omega = \omega_p (1 + 3k^2 \lambda_D^2)^{1/2}$ , and for ions, a resonance would be expected at the frequency of ion-acoustic oscillations  $\omega = k[(\gamma_e T_e + \gamma_i T_i)/M]^{1/2}$ . If, however, the wavelength of the fluctuations is very short in comparison to

the Debye length ( $k\lambda_D \gg 1$ ), the collective plasma effects become relatively unimportant because in this limit the plasma dielectric function approaches unity and the spectral density function reduces to

$$S(\mathbf{k}, \omega) = 2\pi \int F_e(\mathbf{v}) \delta(\omega - \mathbf{k} \cdot \mathbf{v}) d\mathbf{v}, \quad (7)$$

which only depends on the velocity distribution of single uncorrelated electrons.

The form of the spectral density given in Eq. (6) was obtained, independently, by several authors.<sup>14-17</sup> They all assumed, however, that the plasma was collisionless and thus only used the linearized Vlasov equation to calculate the plasma dielectric function. In this approximation, the spectral density function for thermal plasmas is obtained by using a Maxwellian distribution function in the calculation of  $\epsilon(\mathbf{k}, \omega)$ . The resulting ion spectrum for equal ion and electron temperatures is shown in Fig. 1 (the curve due to Salpeter). The ion component is very broad and does not form a true resonance at the ion-acoustic frequency. This occurs because ion-acoustic waves are very strongly Landau damped when electron and ion temperatures are equal.<sup>18</sup>

For most plasmas, the spectrum of fluctuation given by the Vlasov evaluation of Eq. (6) is adequate and has been confirmed by many experiments. See, for example, the extensive reference lists in Refs. 10 and 19. However, if the mean-free path of ion-ion collisions becomes comparable to the wavelength of ion-acoustic fluctuations (i.e.,  $v_{ii}/kC_s \approx 1$ ), then collisions are expected to become important and it is no longer valid to ignore the Balescu-Lenard collision term. In particular, collisions between ions are expected to reduce the efficiency of Landau damping by the introduction of an ion-ion restoring force. As a result, the ion-acoustic resonance should become much more pronounced, even for plasmas with equal electron and ion temperatures.

Finally, it is important to mention that for plasmas which are in thermal equilibrium, the calculation of the density fluctuation spectrum can be greatly simplified by taking advantage of the fact that the fluctuation spectrum is directly related to the electrical conductivity of the plasma. This relation is commonly known as the fluctuation dissipation theorem.<sup>20</sup>

### III. COLLISIONAL KINETIC THEORY

#### A. Balescu-Lenard equation

The electrical conductivity of a highly collisional plasma was first calculated by Kivelson and Dubois.<sup>21</sup> They solved the linearized Balescu-Lenard equation in the limit that the plasma is collisionally dominated, using the Chapman-Enskog technique. This is a perturbational calculation which assumes that the time evolution of the single-particle distribution function is primarily governed by collisions. Thus, the zeroth-order distribution function is obtained from the solution of

$$\left. \frac{\partial f}{\partial t} \right|_{\text{coll}} = 0, \quad (8)$$

while higher-order refinements to  $f$  are obtained by iteration. The convergence of this theory relies on the mean-free path of the plasma particles being much shorter than the wavelength of the plasma fluctuations; therefore, this procedure is only valid if the following condition is satisfied:

$$\frac{k\lambda_D}{g \ln(g^{-1})} \ll 1. \quad (9)$$

Numerical evaluation of the electrical conductivity derived in Ref. 21 and an application of the fluctuation-dissipation theorem yields an ion-acoustic spectrum which is shown in Fig. 2 for various collision frequencies. It is clear that collisions have a significant effect on the shape of the spectrum. Namely, the ion-acoustic resonance becomes pronounced and the zero-frequency entropy fluctuations become apparent. In fact, any collisional kinetic theory should, in the collisionally dominated limit, produce spectra which are qualitatively similar to these. This can be better understood if one examines a fluid model which is formally much simpler and equally valid in the limit of infinite collision frequencies.

In this limit the behavior of the plasma is governed by the usual equation of fluid dynamics

$$\begin{aligned} \frac{\partial \rho}{\partial t} + \nabla \cdot (\rho \mathbf{v}) &= 0, \\ \rho \frac{\partial \mathbf{v}}{\partial t} + \rho(\mathbf{v} \cdot \nabla) \mathbf{v} &= -\nabla p + \nabla \sigma, \\ \rho \frac{\partial \epsilon}{\partial t} + \rho(\mathbf{v} \cdot \nabla) \epsilon &= \vec{\sigma} : \mathbf{d} - \nabla \cdot \mathbf{q}, \end{aligned} \quad (10)$$

where  $d$ ,  $\sigma$ , and  $q$  are the rate of deformation tensor, the stress tensor, and the heat flux, respectively. It is important to note that these equations only describe the time evolution of average macroscopic quantities, which do not fluctuate in equilibrium. It is possible, however, to relate the microscopic fluctuation spectrum to the macroscopic fluid equations by use of the "Onsager's hypothesis of the regression of fluctuations" which states that the correlations  $\langle A(t)A(0) \rangle$  of any microscopic variable  $A$  evolve from time  $t=0$  according to the macroscopic fluid equations.<sup>22</sup>

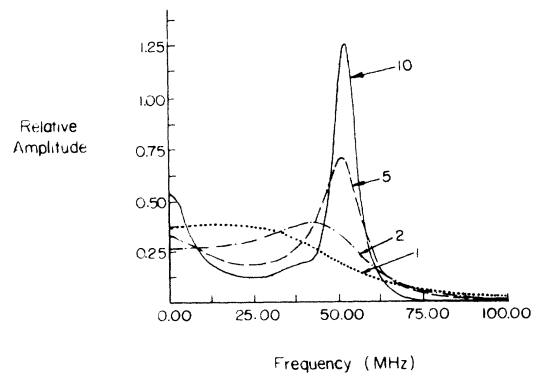


FIG. 2. Shape of the ion-acoustic resonance, as predicted by the Kivelson-Dubois solution of the Balescu-Lenard equation, for various collision frequencies. Curves parametrized by  $v_{ii}/kC_s$ .

Using these equations it can be shown<sup>23</sup> that the spectrum of scattered light from a fluid in thermodynamic equilibrium is given by

$$\frac{\langle \rho(\mathbf{k}, \omega) \rho^*(\mathbf{k}, \omega) \rangle}{\langle \rho(\mathbf{k}) \rho^*(\mathbf{k}) \rangle} = \frac{C_p - C_v}{C_p} \frac{2\kappa k^2 / \rho_0 C_p}{(\kappa k^2 / \rho_0 C_p)^2 + \omega^2} + \frac{C_v}{C_p} \frac{\Gamma k^2}{(\Gamma k^2)^2 + (\omega - C_s k)^2}, \quad (11)$$

where  $C_s$  is the sound speed,  $C_p$  and  $C_v$  are the specific heats at constant pressure and volume,  $\kappa$  is the thermal conductivity, and  $\Gamma$  is the damping coefficient for sound waves:

$$\Gamma = \frac{1}{2} \left[ \frac{4}{3} \frac{n_{sh} + \eta_b}{\rho_0} + \frac{\kappa}{\rho_0} \left( \frac{1}{C_v} - \frac{1}{C_p} \right) \right], \quad (12)$$

and  $\eta_{sh}$  and  $\eta_b$  are respectively the shear and bulk coefficients of viscosity.

An examination of this equation reveals that the fluctuation spectrum of a fluid plasma is composed of two distinct components: one at zero frequency due to nonpropagating entropy fluctuations and one at the ion-acoustic frequency due to propagating pressure fluctuations. The width of the two resonances is determined, respectively, by the thermal conductivity and the ion-acoustic damping coefficient. Both of these parameters decrease with increasing collision frequency. Thus, the fluid model qualitatively produces the type of spectra predicted by the Kivelson-Dubois calculation and expected of all collisional kinetic theories in the limit of high-collision frequencies.

### B. BGK model

Another very successful treatment of collisional plasmas is the Bhatnagar-Gross-Krook<sup>1</sup> (BGK) theory which employs a pseudo-phenomenological collision term that satisfies the basic requirement that particle number, momentum, and energy be conserved in any collisional interaction. In the BGK model, the time evolution of the one-particle distribution function due to two-particle collisions is governed by

$$\begin{aligned} \frac{\partial}{\partial t} f(\mathbf{v}, \mathbf{r}, t) + \mathbf{v} \cdot \frac{\partial}{\partial \mathbf{r}} f(\mathbf{v}, \mathbf{r}, t) - \frac{e\mathbf{E}}{m} \cdot \frac{\partial}{\partial \mathbf{v}} f(\mathbf{v}, \mathbf{r}, t) \\ = - \frac{n(\mathbf{r}, t)}{\sigma} f(\mathbf{v}, \mathbf{r}, t) + \frac{n^2(\mathbf{r}, t)}{\sigma} \Phi(\mathbf{v}, \mathbf{r}, t), \end{aligned} \quad (13)$$

$$\Phi = \left[ \frac{m}{2\pi k_B T(\mathbf{r}, t)} \right]^{3/2} \exp \left[ - \frac{m}{2k_B T(\mathbf{r}, t)} [\mathbf{v} - \mathbf{u}(\mathbf{r}, t)]^2 \right],$$

where  $\mathbf{u}(\mathbf{r}, t)$  and  $T(\mathbf{r}, t)$  are the flow velocity and temperature at  $x$  and  $t$  and where  $n(\mathbf{r}, t)/\sigma$  is the effective collision frequency.

The first part of the collision term  $n(\mathbf{r}, t)f(\mathbf{v}, \mathbf{r}, t)/\sigma$  corresponds to the rate at which particles leave a particular velocity range  $\mathbf{v}$  at a position  $\mathbf{r}$  and  $t$ . The second term  $n^2(\mathbf{r}, t)\Phi(\mathbf{v}, \mathbf{r}, t)/\sigma$ , on the other hand, corresponds to the rate at which particles are reintroduced into the same

velocity, position, and time range, except that now it is assumed that these particles have already relaxed to the local equilibrium distribution and thus are emitted with a Maxwellian velocity distribution centered about the local flow velocity  $\mathbf{u}(\mathbf{r}, t)$ .

For small deviations from equilibrium, the collision term can be linearized; this form of the BGK collision term was employed by Leonard and Osborn<sup>6</sup> and Theimer and Theimer<sup>5</sup> to calculate the electron density fluctuation spectrum in equilibrium plasmas. Leonard and Osborn used a stochastic approach,<sup>24</sup> while Theimer and Theimer used the Fourier-Laplace method to calculate the electrical conductivity and subsequently the fluctuation spectra via the fluctuation-dissipation theorem. Theimer and Theimer's calculations were, however, simplified since they assumed an isothermal plasma (i.e.,  $T = T_0$ ).

In this work we extended Theimer and Theimer's calculations by removing the isothermal restriction. Figure 3 displays the results of such a calculation near the ion-acoustic frequency for both the general and isothermal cases. It is clear from these results that both the general and isothermal cases show strong collisional modification of the ion-acoustic spectrum, however, the isothermal simplification omits important features of the fluctuation spectra. If the local temperature is included, then the ion-acoustic resonance shifts to a frequency corresponding to the adiabatic sound velocity and the zero-frequency resonance appears, signifying the presence of nonpropagating entropy fluctuations. In general, the qualitative behavior of the BGK model is comparable to that obtained from the Balescu-Lenard equation.

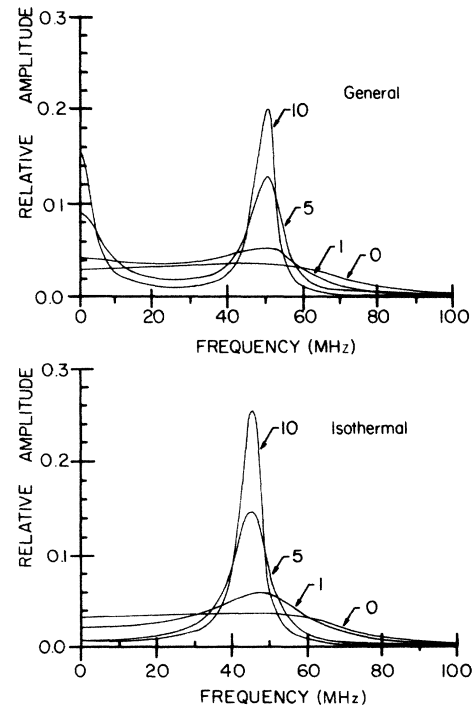


FIG. 3. Ion-acoustic spectra for a 2 eV argon plasma for various collision frequencies ( $\nu_{ii}/kC_s$ ) as predicted by the general and isothermal BGK models.

### C. Fokker-Planck model

The Fokker-Planck equation, commonly used in calculating transport quantities, is also useful in calculating the fluctuation spectra of collisional plasmas. Such a calculation was used by Grewal<sup>4</sup> where he assumed that the effect of collisions on the time evolution of a single-particle distribution function is the same as that which a particle experiences when undergoing Brownian motion. The Fokker-Planck collision term corresponding to Brownian motion may be written as<sup>25</sup>

$$\left[ \frac{\partial}{\partial t} \mathbf{v} \cdot \frac{\partial}{\partial \mathbf{r}} + \frac{e}{m} \mathbf{E} \cdot \frac{\partial}{\partial \mathbf{v}} \right] f(\mathbf{r}, \mathbf{v}, t) = \nu \frac{\partial}{\partial \mathbf{v}} \left[ \mathbf{v} + \frac{T}{m} \frac{\partial}{\partial \mathbf{v}} \right] f(\mathbf{r}, \mathbf{v}, t), \quad (14)$$

where  $\nu$  is the effective collision frequency. The first term corresponds to collisional friction, while the second term represents diffusion in velocity space due to collisions.

Grewal solved this equation for both electrons and ions using a Green's function approach and calculated the electron density fluctuation spectrum with a method equivalent to the fluctuation-dissipation theorem. In Fig. 4 we show a calculation of the ion-acoustic fluctuation spectra for different values of the collision frequency. It is obvious from these spectra that in the limit of high collision rates, the ion-acoustic resonance is completely damped out, while at the same time the zero-frequency fluctuations are predicted to grow. This is in direct contradiction to the predictions of the BGK and Balescu-Lenard collision models and is caused by the fact that the Fokker-Planck collision term for a Brownian particle as given by Eq. (14) conserves neither momentum nor energy. As a result, this form of the Fokker-Planck collision term is only appropriate for treating collisions which transfer negligible amounts of momentum and energy between colliding species, as is the case for electron-neutral collisions in weakly ionized plasmas.

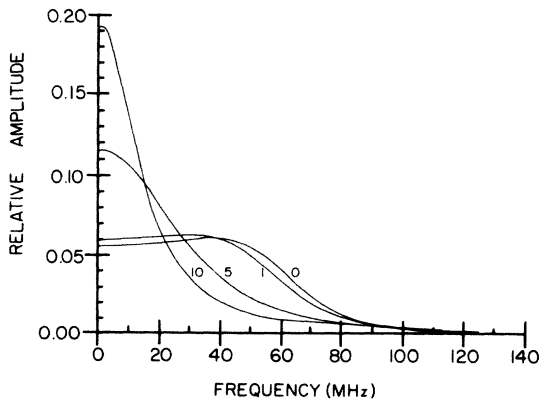


FIG. 4. Fokker-Planck calculation of the Ar (2 eV) ion-acoustic resonance which is parametrized by  $\nu_{ii}/kC_s$ .

### D. Generalized Langevin equation

With the exception of the BGK theory, which does not possess a formal foundation, all of the models discussed so far are formally based on the assumption that the plasma parameter  $g=1/n\lambda_D^3$  is small. There exists, however, a kinetic formalism which does not rely on expansions in the plasma parameter but instead casts the basic kinetic equations in the form of the generalized Langevin equation. This formalism is commonly referred to as the projection operator technique, developed by Zwanzig<sup>26</sup> and Mori<sup>27</sup> for the study of nonequilibrium statistical mechanics.

By use of projection-operator techniques, Mori<sup>27</sup> was able to show that the time evolution of an arbitrary set of dynamic variables  $\mathbf{A}=(A_1, \dots, A_n)$  of a many-body system can be put into the form of a generalized Langevin equation, as given by

$$\begin{aligned} \frac{d\mathbf{A}(0)}{dt} &= i\mathbf{\Omega} \cdot \mathbf{A}(t) - \int_0^t d\tau \Phi(\tau) \cdot \mathbf{A}(t-\tau) + f(t), \\ f(t) &= \exp[i\tau(1-P)L] i(1-P)L A(0), \\ \Phi(\tau) &= \langle f(\tau) f^*(0) \rangle \langle A(0) A^*(0) \rangle^{-1}, \\ i\mathbf{\Omega} &= \langle \dot{A}(0) A^*(0) \rangle \langle A(0) A^*(0) \rangle^{-1}, \end{aligned} \quad (15)$$

where  $f(t)$  is the microscopic random force acting on  $A$ ,  $\Phi(\tau)$  corresponds to the system dissipation due to the random force, and  $\mathbf{\Omega} \cdot \mathbf{A}$  gives the time evolution of the  $A$  due to the evolution of the macroscopic system variables. The projection operator  $P$  is defined by its action on an arbitrary dynamic variable  $B$  as

$$PB \equiv \langle BA^*(0) \rangle \langle A(0) A^*(0) \rangle A(0), \quad (16)$$

and  $L$  is the Liouville operator,  $L=i\{H, \}$ .

Equation (15) is an exact expression for  $A(t)$  and its solution would still require one to solve the many-body problem. However, the real quantity of interest is the correlation matrix  $\mathcal{C}(t)$  which can be calculated fairly readily since the equation which governs it

$$\dot{\mathcal{C}}(t) - i\mathbf{\Omega} \cdot \mathcal{C}(t) + \int_0^t d\tau \Phi(\tau) \cdot \mathcal{C}(t-\tau) = 0 \quad (17)$$

is much simpler in the sense that all of the system dynamics are solely governed by the damping matrix  $\Phi(t)$  which is usually successfully modeled by use of simple physical arguments.

An application of this technique to the study of density fluctuations in a plasma was first made by Linnebur and Duderstadt.<sup>2</sup> They used a generalized version of Eq. (15) represented by

$$\begin{aligned} \dot{\mathcal{C}}(p) - i \int d\mathbf{p}' \mathbf{\Omega}(p, p') \cdot \mathcal{C}(p', t) \\ + \int_0^t d\tau \int d\mathbf{p}' \Phi(p, p', \tau) \cdot \mathcal{C}(p', t-\tau) = 0 \end{aligned} \quad (18)$$

to generate a set of coupled equations for the time evolution of the electron density fluctuation spectrum. These equations were solved by assuming that the static correlation function  $\langle A(0) A(0) \rangle$  for the electrons and ions could be calculated from the Debye-Hückel pair correlation function and that the damping kernels  $\Phi$  decayed exponentially in time.

Numerical evaluation of the Linnebur-Duderstadt solutions, in this work, showed that in the short-wavelength limit the solutions were well behaved and in agreement with the numerical calculations presented in Ref. 2. However, for long-wavelength fluctuations, such as the ones sampled by small angle laser scattering experiments, the calculated fluctuation spectrum became negative valued and thus unphysical. This result led to the discovery of an error in the original work of Linnebur and Duderstadt<sup>28</sup> which if corrected produced physically acceptable results for both long- and short-wavelengths. Figure 5 shows such calculations for the ion-acoustic spectra of a (2 eV) argon plasma with various effective collision frequencies. These results look very similar to the Fokker-Planck calculations in the sense that the ion-acoustic fluctuations are totally damped out in the highly collisional regime. Such behavior is suggestive of equations which do not conserve energy or momentum. In fact, it was pointed out in Ref. 29 that the Linnebur-Duderstadt model is not energy conserving.

#### IV. EXPERIMENTAL PROCEDURE

##### A. Plasma source

The testing of the various collisional theories previously discussed requires the use of a very dense, low-temperature plasma which is in kinetic thermodynamic equilibrium and for which the plasma density, temperature, and impurity content are accurately known. These requirements were satisfied by the use of a pulsed arc, designed to produce plasmas with  $n=10^{17} \text{ cm}^{-3}$ ,  $T=2 \text{ eV}$  which last for about  $100 \mu\text{sec}$ . The arc was also made capable of high repetition rates (0.5 Hz) in order to allow for integration of the scattering signals cumulatively over many shots.

The arc consisted of a quartz tube ( $r=2.3 \text{ cm}$ ,  $l=22 \text{ cm}$ ) mounted between two copper-tungsten alloy electrodes which were fed by a  $1200 \mu\text{F}$  capacitor bank charged to 1–2 kV. To produce a relatively flat current pulse over the time of the discharge, and hence a quiescent plasma, the capacitor bank used to drive the arc was

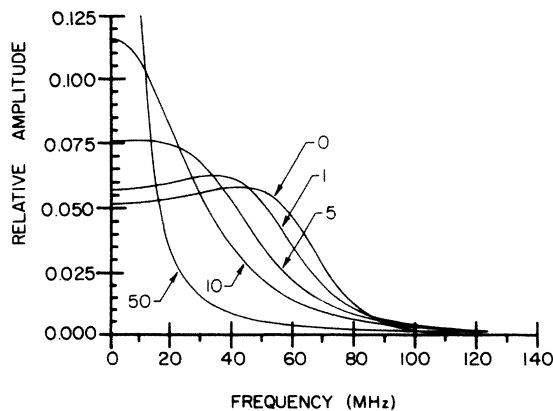


FIG. 5. Ion-acoustic spectra for Ar (2 eV) calculated from Linnebur-Duderstadt model. Parametrized by  $\nu_{ii}/kC_s$ .

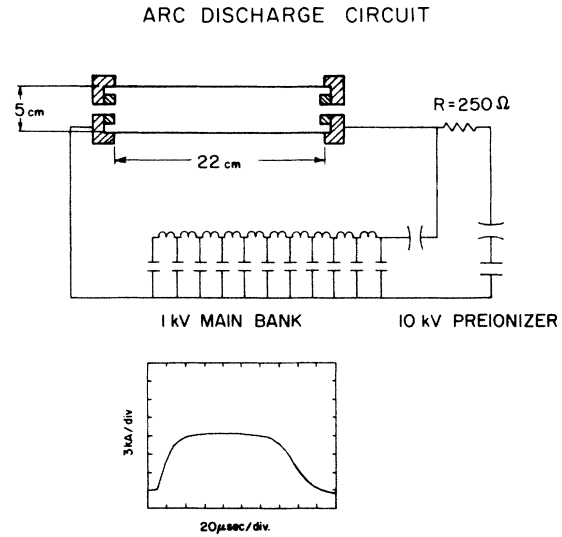


FIG. 6. Schematic of the arc discharge circuit with a sample of a typical discharge current profile.

constructed as a lumped delay line which has the characteristic of producing square discharge pulses. A schematic of the capacitor bank circuit and a typical discharge pulse are shown in Fig. 6.

In normal operation, the chamber was filled to 1–7 Torr with helium or argon gas and discharge currents of about 10–25 kA produced plasmas with densities and temperatures of about  $10^{16}$ – $10^{17} \text{ cm}^{-3}$  and 2–4 eV. For scattering measurements, the plasma collisionality was maximized by operating the arc at the highest pressure (3 Torr for Ar and 7 Torr for He) and the lowest bank voltage (1500 V) consistent with stable plasma discharges. This produced plasmas with 1.95 eV and  $10^{17} \text{ cm}^{-3}$  for argon. The corresponding degree of ionization was near 100% in argon and about 50% in helium.

The electron density in the arc plasma was determined from axial line density measurements made through openings in the electrodes with a quadrature HeNe laser interferometer. In determining the density, it was assumed that the axial line density was directly proportional to the length of the plasma column. This was verified by measuring the radial line density and finding it independent of axial position. From these measurements, the electron density was found to be a smooth function of time, as shown in Fig. 7, roughly following the profile of the current pulse. Measurements at various radial positions also showed that the plasma density was relatively flat across the diameter of the discharge tube, as seen in Fig. 8, indicating a very uniform arc discharge.

Electron temperatures of the arc plasma were determined by measuring the ratio of spectral line intensities from successive ionization stages of the same ionic species.<sup>30</sup> In particular, argon plasma temperatures were determined from the Ar II (3350.9 Å) and Ar III (3344.7 Å) lines. These lines were chosen since they are well isolated and their intensity ratios are very sensitive to tem-

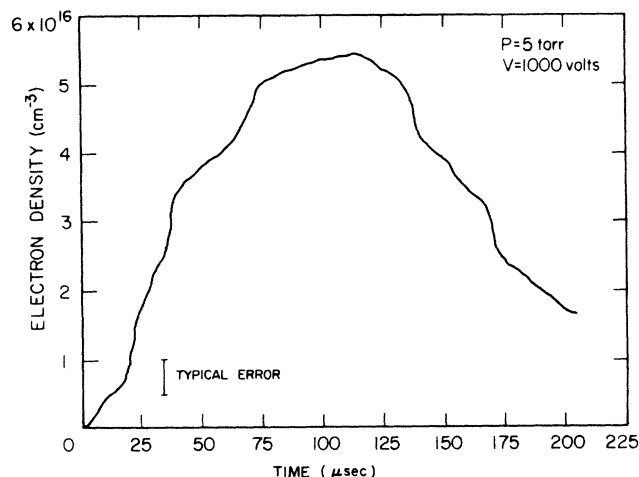


FIG. 7. Typical time history of the electron density in a He plasma. Measured by a HeNe quadrature interferometer.

perature in the 2 eV range.<sup>31</sup> Furthermore, the very small (5 Å) wavelength separation of the lines made relative intensity calibration of the spectrometer unnecessary. These lines were also used to measure the temperature of helium plasmas containing argon as a trace impurity (helium lines were not chosen because it was difficult to find helium lines that were as sensitive and as easily measurable in this temperature range). Some typical temperature measurements are displayed in Fig. 9, while a radial temperature scan showing a very flat temperature profile is displayed in Fig. 10. Errors in the temperature measurements were primarily due to uncertainties in the transition probabilities of the argon lines (50%) and in the calculation of the upper-state population densities of the Ar III line (30%). Nevertheless, the error in determining the temperature

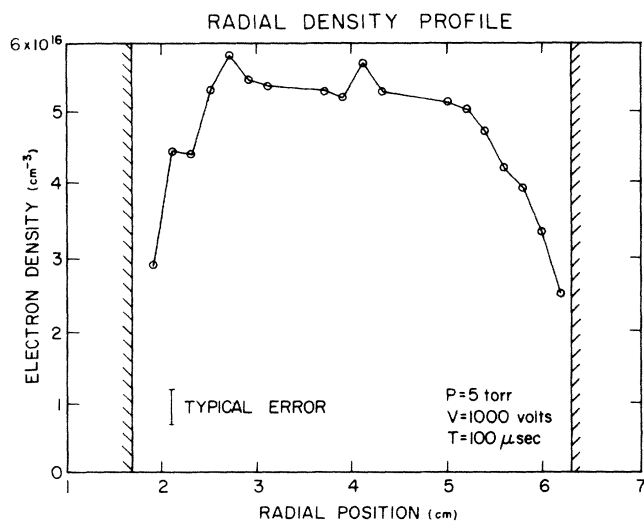


FIG. 8. Typical radial density profile of the arc plasma. Shown for He discharges.

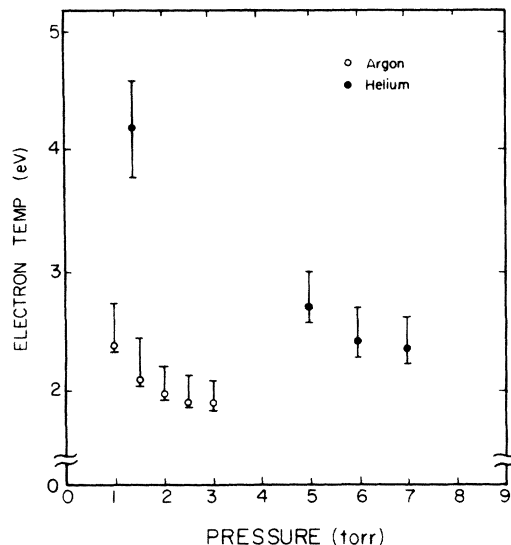


FIG. 9. Electron temperature of argon and helium plasmas as a function of fill pressure. Measured from the ratio of spectral line intensities.

was small (10%) due to the sensitivity of the line ratios to temperature.

Impurity contamination of the plasma was checked spectroscopically by observing the prominent emission lines of ionized electrode, wall, and pump oil atoms (Cu, W, Zn, Si, O, C). Only electrode impurities were found, by the detection of both copper (Cu II 2770 Å, Cu II 2545 Å) and tungsten (W II 2030 Å) lines. Using the ratio of impurity and nonimpurity line intensities and the Saha equation, it was possible to set an upper limit of 1.8% and 1.3% on the impurity concentration of copper and tungsten, respectively.

The stability properties of the plasma were checked by use of high-speed photography, inductive probes, and electric Langmuir probes. Framing camera photographs with

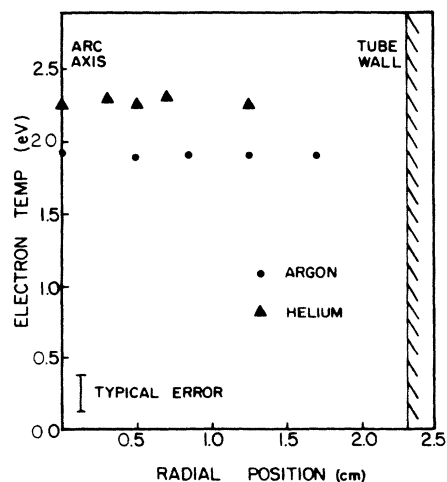


FIG. 10. Radial distribution of temperature in argon and helium discharges.

exposure times as short as 5 nsec showed the plasma to be stable, uniform, and reproducible in both helium and argon discharges in the 1–7 Torr and 1–3 Torr pressure ranges, respectively. Magnetic probe measurements showed that there were two basic modes of operation of the arc discharge. At early times ( $\tau < 30$  sec), the bulk of the current was concentrated in the central region of the arc (within the radius of the electrodes  $r < 0.5$ ), while at later times ( $\tau > 50$  sec) the current distribution diffused outward until the current density was constant across the arc radius. Conveniently, the uniform current density mode of operation would last for times longer than 50  $\mu$ sec, thus permitting adequate time for scattering experiments. Finally, electric probes confirmed the results of the previous diagnostics by showing that the plasma was very uniform and quiescent in the sense that the measured floating potential showed no signs of large-scale fluctuations and that the gradient in the potential was a smooth function of axial position.

### B. Laser scattering setup

Scattering measurements with long-wavelength lasers from dense low-temperature plasmas are generally very difficult to perform since whenever the input laser power is sufficiently intense to produce a discernible scattering signal, it is also sufficiently intense to perturb the plasma by heating it. In this experiment, the problem of heating the plasma was overcome by the use of a heterodyne technique<sup>32,33</sup> which is capable of boosting the detected signal many orders of magnitude; as a result, it permits the use of a relatively low-power laser (200 W) which does not perturb the plasma.

A schematic of the heterodyne scattering configuration is shown in Fig. 11. First, a small fraction of the main laser beam ( $TEM_{00}$ ,  $p = 100$ – $200$  watts,  $\tau = 100$   $\mu$ sec) is split off to form a local oscillator beam and, subsequently, the main and local oscillator beams are focused into the

plasma with a 10-cm-focal-length lens. Any light that is scattered out of the main beam and into the solid angle subtended by the local oscillator beam is imaged onto a liquid-helium cooled Ge:Cu detector. The nonlinear mixing of the scattered and local oscillator beams produce a detected photocurrent, which contains the plasma fluctuation spectra. In particular, the photocurrent can be expressed as

$$I_0(t) = \frac{\eta G e}{h\nu} \{ P_s + P_{LO} + 2\zeta [P_s(\omega)P_{LO}]^{1/2} \cos(\omega t) \}, \quad (19)$$

where  $P = c(EE^*/8\pi)$  is the average power of the individual fields,  $\eta$  and  $G$  are the detector quantum efficiency and gain,  $\omega$  is the fluctuation frequency, and  $\zeta$  is the mixing efficiency which measures the extent to which the two radiation fields are in phase over the surface area of the detector. The form of this photocurrent shows that mixing the scattered light with a local oscillator beam produces a signal that is composed of two distinct components: a slowly varying (frequency  $\approx 1/\text{laser pulse length}$ ) average power envelope that is due to the local oscillator and scattered light beams ( $P_s + P_{LO}$ ); and a high-frequency beat (i.e., heterodyne) term which contains the plasma fluctuation spectrum  $[(P_s P_{LO})^{1/2} \cos \omega t]$ . The heterodyne term is in the radio frequency range in this work. Consequently, it is easily differentiated from the low-frequency average power terms and its spectrum is analyzed at high resolution ( $\Delta f = 6$  MHz) by the use of a scannable electronic filter. In addition, the capability to separate the heterodyne term from the very large average power terms permits scattering measurements in high stray light environments, as is the case for small angle scattering. The stray light, not being frequency shifted by the scattering process, only contributes to the average power terms which are easily filtered out.

### SCATTERING GEOMETRY

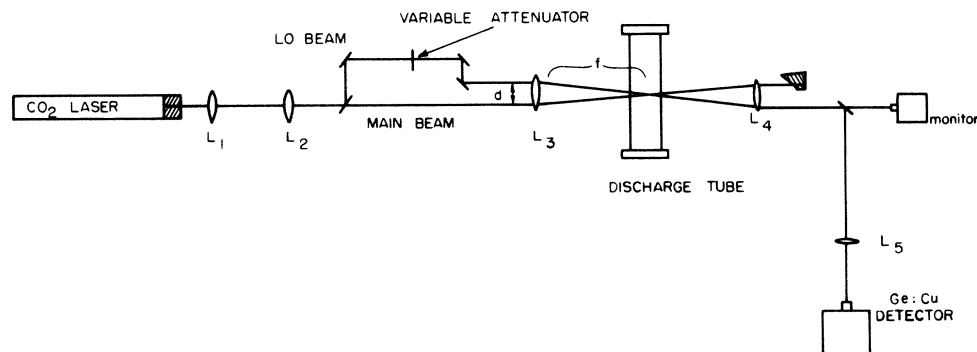


FIG. 11. Diagram of the optical system and scattering geometry.

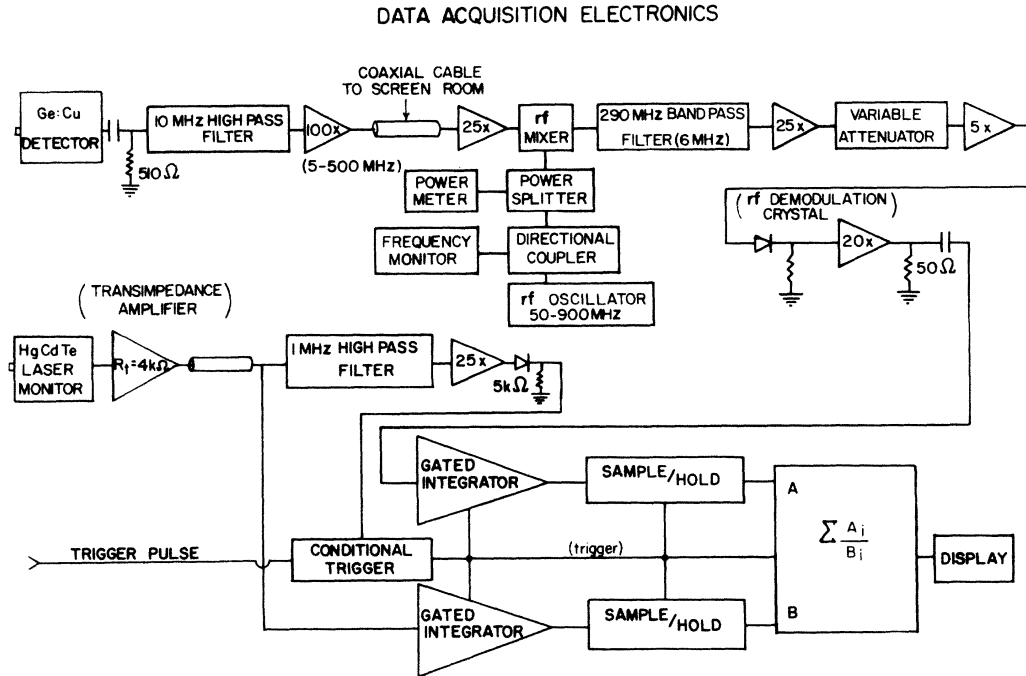


FIG. 12. Schematic of the data acquisition electronics.

### C. Data acquisition system

To recover the density fluctuation spectrum from the detector photocurrent, an elaborate system of electronics was developed which could perform the required analysis. A general schematic of the system is displayed in Fig. 12. First, the detected photocurrent ( $I=0.1-1 \mu\text{A}$ ) is filtered with a 10 MHz high-pass filter to remove the low-frequency power envelope of the local oscillator. The much higher frequency (10–300 MHz) scattered signal is allowed to pass through and is amplified by high-frequency low-noise amplifiers (500 MHz bandwidth,  $NF \approx 2.5$ ). Subsequently, the high-frequency signal is mixed with a rf local oscillator to produce an intermediate-frequency (IF) difference signal centered at 290 MHz and having a bandpass of 6 MHz. Only those signals which differ from the rf local oscillator by 290 MHz are permitted to pass through, thus it is possible to scan across the frequency spectrum of the detector signal by simply changing the frequency of the rf local oscillator. Finally, the intensity of the IF signal is detected with a square law crystal and integrated with a gated integrator.

It is necessary to square and integrate the detector signal because it is the mean-square detector current which is actually related to the average scattering intensity, as can be seen from Eq. (19). The mean-square detector current is, however, also proportional to the local oscillator laser power; therefore, in order to remove this dependency, the local oscillator power is monitored by a separate detector and integrated with an identical gated integrator to produce a normalization signal. The two signals are then stored in a low-leakage sample and hold circuit until they

can be analyzed. Normally data is averaged over many shots; thus, the data unit normalizes each individual detector signal and then adds it to the sum of all of the preceding ones. The resultant output signal displayed by the data acquisition system is then given by

$$V_s(f_0) = \sum_i \frac{\beta}{\langle P_{LO} \rangle_i} \times \int_0^t \left[ \int_{-\infty}^{\infty} F(f) C(f-f_0) I_{D_i}(f) df \right]^2 dt, \quad (20)$$

where the sum is over individual plasma shots,  $F(f)$  is the frequency response of the detector and the detection system,  $C(f-f)$  is the instrument function of the IF filter, and  $\beta$  represents all of the conversion and system gain factors. In general, the scattering spectrum and frequency response of the system are fairly constant over the detection bandwidth. Thus, it is possible to reduce Eq. (20) to

$$V_s(f_0) = \sum_i \frac{\langle I_D(f_0) \rangle_i}{\langle P_{LO} \rangle_i} \beta F^2(f_0) \left[ \int_{-\infty}^{\infty} c(f-f_0) df \right]^2, \quad (21)$$

where  $I_D$  is the total mean-square detector current.

This system works very well unless the laser should mode beat during the course of a data shot. Mode beating produces signals which are in the same frequency range as the scattered signals but many orders of magnitude

greater in intensity. Even one such mode beating signal is sufficient to skew the data tremendously. The recording of mode beating signals is prevented by monitoring the high-frequency spectrum of the laser monitor signal. If a mode beating signal is detected, a conditional circuit inhibits the data acquisition unit so that it does not sample the contents of the sample and hold circuit for that particular shot. In addition, another conditional circuit monitors the plasma discharge current and rejects the scattering data from abnormal discharges.

## V. SCATTERING RESULTS

### A. Scattering procedure

In practice, the mean-square current analyzed by the data-acquisition unit is composed of not only the scattering signal but also of signal currents from various noise sources in the detection system. The most important of these is the shot noise<sup>34</sup>

$$\langle I_{\eta}^2 \rangle = \frac{4e^2 G^2 \eta P_{LO} \Delta f}{h \nu} \quad (22)$$

generated in the detector by the laser local oscillator. In fact, under the conditions of this experiment the shot noise amplitude is greater than that of the scattered signal. However, this did not pose any problem in measuring the scattered spectra because the signal-to-noise ratio for heterodyne detection<sup>35</sup>

$$(S/N) + \frac{(1+f \Delta \tau)^{1/2}}{1 + \frac{2h \nu \Delta f}{\eta \xi^2 P_s}} \quad (23)$$

can be much greater than one, provided that the integration time  $\tau$  is made long enough. Physically, Eq. (23) corresponds to the fact that long observation times and large bandwidths permit accurate determination of the mean values of both the signal and noise amplitudes in spite of statistical fluctuations about their respective means.

In this experiment the frequency spectra of the scattered light was extracted from the noise by a two-step process. First, the total mean-square detector photocurrent  $\langle I^2 \rangle = \langle I_s^2 \rangle + \langle I_n^2 \rangle$  was integrated and normalized as discussed in the previous section. Then, an additional measurement was made under identical conditions except that the main laser beam, but not the LO beam, was physically obstructed to prevent a scattering contribution to the detector photocurrent. This produced a signal identical to the previous measurement except that this time it was only due to the shot noise induced by the local oscillator,  $\langle I^2 \rangle = \langle I_n^2 \rangle$ . To determine the scattering amplitude the two signals were subtracted and the difference normalized by the noise signal. Using Eqs. (19), (21), and (22) it can be shown that this results in a quantity

$$\frac{V_s - V_{ns}}{V_{ns}} = \frac{\eta \xi^2 \sum_i \langle P_s \rangle_i}{2h \nu \Delta f}, \quad (24)$$

which is directly proportional to the average scattered power  $\langle P_s \rangle$  and only depends on constant system parameters, thus directly yielding the average scattering ampli-

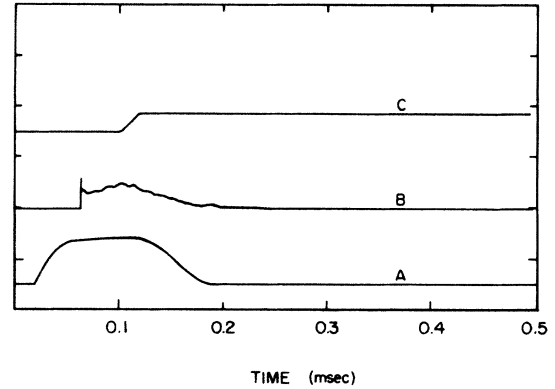


FIG. 13. Standard timing synchronization of the gated integrator. The integrator output (trace *c*) is held constant after the integration period by a sample and hold circuit. Trace *B* is the temporal laser pulse profile and trace *A* is the arc current pulse shape.

tude at the selected sample frequency. The complete spectrum is obtained by repeating this process throughout the necessary frequency range.

For the data presented in this paper, the integration time per shot was set at 40  $\mu$ sec, and 50 scattering and 50 nonscattering shots were taken for each data point. Figure 13 shows the standard timing sequence of the gated integrator with respect to the discharge current pulse.

### B. Effects of the discharge current on the scattering spectra

Initial scattering measurements were made in argon plasmas and the observed spectra showed substantial peaking near the ion-acoustic frequency. This is expected for collisional plasmas, but similar behavior can also be produced by current-driven ion-acoustic waves.<sup>16</sup> To determine if the observed spectra were due to current-driven ion-acoustic waves, the scattering spectrum was measured for both  $k$  parallel and perpendicular to the discharge current. The switching from one case to the other was accomplished by a 90° rotation of the arc plasma about the incident light-beam axis perpendicular to the current. This produced the required change in the orientation of the scattering vector with respect to the current without actually changing the optical alignment of the system, thus allowing both orientations to be sampled in a single scattering run. The results of such a measurement from an argon plasma ( $T = 1.95$  eV,  $n = 1 \times 10^{17}$  cm<sup>-3</sup>) are shown in Fig. 14 from which it can be seen that fluctuations with  $\mathbf{k} \perp \mathbf{J}$  are enhanced by about 30% over the fluctuations with  $\mathbf{k} \parallel \mathbf{J}$ . This relatively small enhancement level suggests that ion-acoustic waves parallel to the current are weakly driven, and are thus uncoupled from fluctuations perpendicular to the current. As an additional test, the  $\mathbf{k} \parallel \mathbf{J}$  scattering spectrum was also measured both during the discharge, when the current was about 17 kA, and during the afterglow, when the current had fallen to zero and was incapable of driving instabilities. In this measurement, the integration time per shot was reduced to about 25  $\mu$ sec in order to limit the integra-

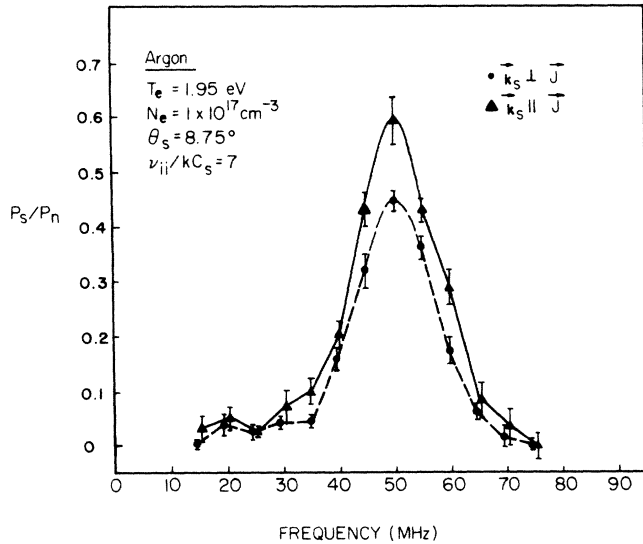


FIG. 14. Scattered ion-acoustic spectra for the two cases of  $\mathbf{k} \perp \mathbf{J}$  and  $\mathbf{k} \parallel \mathbf{J}$  which demonstrate the effect of the discharge current.

tion over rapidly changing plasma conditions in the afterglow plasma. Figure 15 displays the results of these measurements which show that the zero current spectrum is shifted to lower frequencies due to lower plasma temperatures (1.5 eV) in the afterglow and that the zero current fluctuation level was about 60% less than during the discharge. After correcting for the lower plasma density and lower laser absorption in the afterglow plasma, the

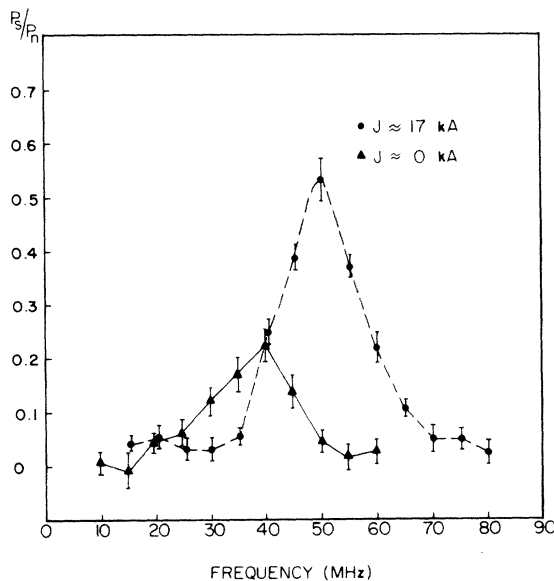


FIG. 15. Scattering spectra for a 2 eV argon plasma with  $\mathbf{k} \parallel \mathbf{J}$  for both zero and full discharge current. The enhancement of the spectra for  $J = 17$  kA is comparable to the enhancement shown in Fig. 14 if corrections are made for lower plasma density and lower laser absorption in the afterglow plasma.

enhancement level was determined to be about 33% which compares very favorably with the previous measurement. This proved that the ion-acoustic waves parallel to the current are not coupled to the current; thus, parallel fluctuations are only due to thermally excited waves.

### C. Final data

A comparison of the theories discussed in Sec. III with the scattering results required that the data originate from thermal fluctuations. Final data were, therefore, taken with  $\mathbf{k} \perp \mathbf{J}$ . Specifically, scattering spectra from both helium (2.3 eV,  $1 \times 10^{17} \text{ cm}^{-3}$ ) and argon (1.95 eV,  $1 \times 10^{17} \text{ cm}^{-3}$ ) plasmas were each measured at scattering angles of  $8.75^\circ$  and  $4.7^\circ$ . These spectra are shown in Figs. 16 and 17. As expected, they show substantial enhancement and narrowing, with the peak amplitudes being about 10 times the predicted amplitudes of collisionless theory. Each data point corresponds to a scattering signal averaged over fifty discharges of the arc and the error bars are derived from the standard deviation of the mean.

Another item of interest is the degree to which unlike ions couple through collisions. To study this, additional scattering measurements were made in composite helium-argon plasmas. The resultant spectra for different Ar:He mixtures (0.2:6.8; 0.5:6.5) are, respectively, shown in Figs. 18 and 19. Strong coupling between helium and argon ions is evident from the fact that the observed peaks are located at the ion acoustic frequencies which correspond to the average mass of the Ar:He mixtures.

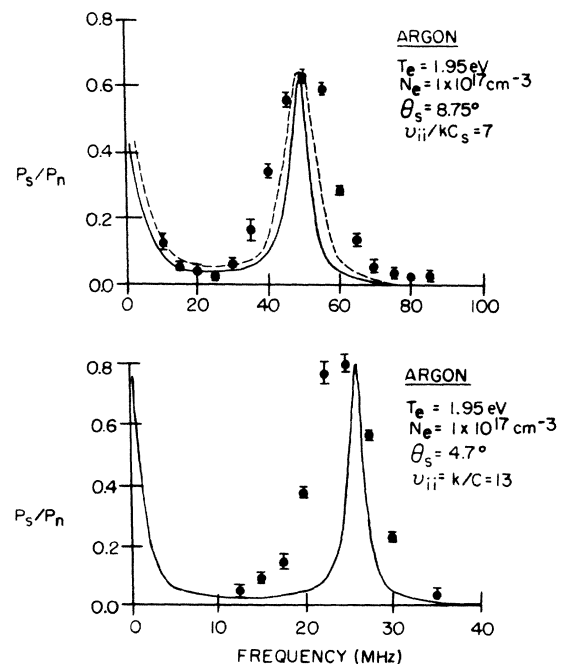


FIG. 16. Scattered light spectra in argon for  $4.7^\circ$  and  $8.75^\circ$  scattering angles. Calculated curves are due to the BGK theory (Refs. 1, 5, and 31). The dashed curves are due to the BGK theory convoluted with the finite resolution of the experiment.

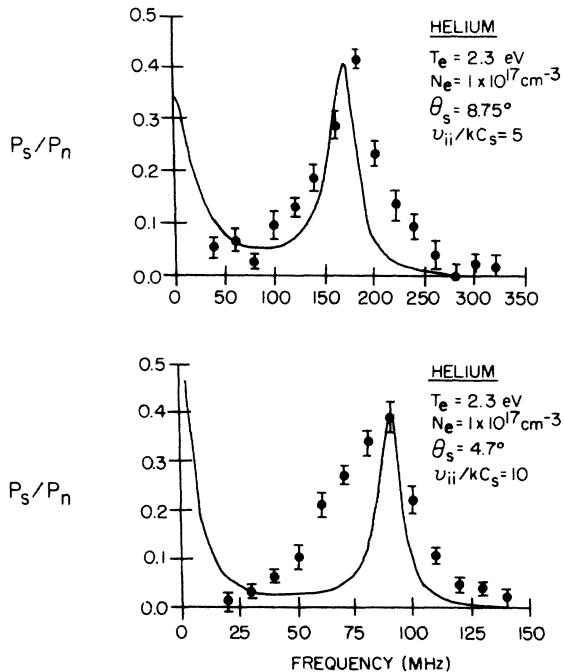


FIG. 17. Scattered light spectrum in helium for 4.7° and 8.75° scattering angles. Theory curves are as in Fig. 16.

## VI. INTERPRETATIONS

Even though the observed enhancement of the ion-acoustic resonance is interpreted as evidence of collisional plasma behavior, it is important to rule out the possibility that such enhancement could also have been produced by collisionless mechanisms. Most importantly, reduction of Landau damping due to unequal electron and ion temperatures and nonthermal excitations due to the discharge current could have both produced the observed spectra.

Enhancements of the spectra due to current-driven ion-

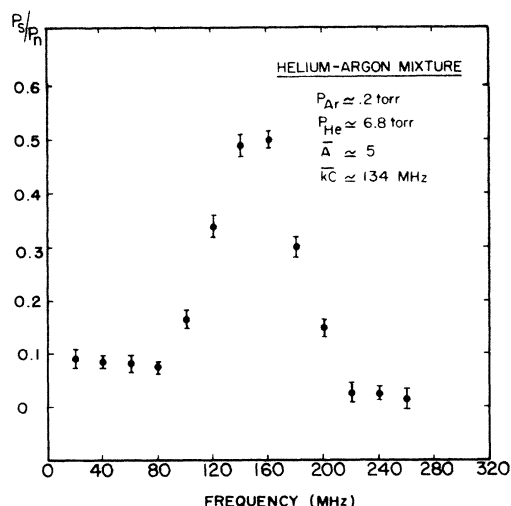


FIG. 18. Scattered light spectrum from a composite HeAr plasma. Mixing ratio He:Ar = 34:1.

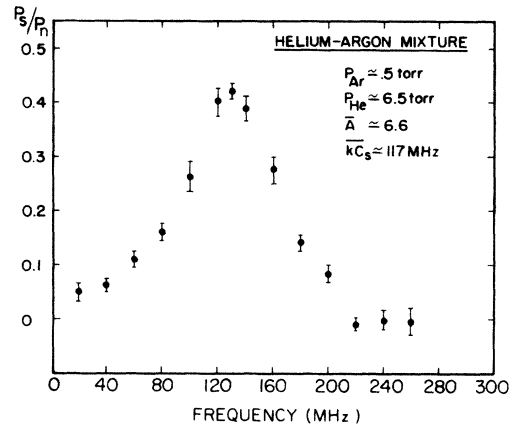


FIG. 19. Scattered light spectrum from a composite HeAr plasma. Mixing ratio He:Ar = 13:1.

acoustic waves has already been shown by experiment to be very unlikely for scattering data obtained with  $\mathbf{k} \perp \mathbf{J}$ . To further remove any doubts about this, it is also possible to show that the observed difference between the  $\mathbf{k} \parallel \mathbf{J}$  and  $\mathbf{k} \perp \mathbf{J}$  spectra is in accordance with theoretical estimates. In particular, the degree to which the fluctuation spectrum is enhanced in the presence of an electron drift current can be estimated by considering the behavior of the spectral density function in the vicinity of a normal mode of the plasma. At a normal mode resonance  $S(\mathbf{k}, \omega)$  depends very strongly on the form of the single-particle distribution function as<sup>36</sup>

$$S(\mathbf{k}, \omega) \propto - \frac{f(\omega/k)}{\left. \frac{\partial f(v)}{\partial v} \right|_{v=\omega/k}} \delta(\omega - \omega_0). \quad (25)$$

Thus, enhancements due to a drift current in an equilibrium plasma are estimated by evaluating Eq. (25) for both an equilibrium Maxwellian distribution and for a Maxwellian centered about the electron drift velocity  $v_d$ . The ratio of the two expressions yields

$$\frac{S(\mathbf{k}, \omega; v_d)}{S(\mathbf{k}, \omega; v_d=0)} = \frac{C_s}{C_s - v_d}, \quad (26)$$

which gives an approximation level of the enhancement of  $S(\mathbf{k}, \omega)$  due to the electron drift current.

For the plasmas used in this work, the drift velocity was approximately 20% of the ion-acoustic velocity; thus, the fluctuation levels parallel to the current should have been enhanced by about 25% over thermal levels. The measured enhancement level of 33% agrees to within experimental error with the predicted value, thereby confirming the previous assumption that the scattered spectra measured with  $\mathbf{k} \perp \mathbf{J}$  are not enhanced by virtue of the discharge current.

Reduction of Landau damping due to unequal electron and ion temperatures is also very unlikely because the collisional equilibration time between ions and electrons (70

nsec) is much shorter than the arc duration (100  $\mu$ sec). As a result, electrons and ions can easily reach equilibrium among themselves within the 100  $\mu$ sec duration of the plasma. Also, it is evident from the solution of Eq. (6) that the electron temperature would have to be about eight times that of the ion temperature in order for the collisionless result to qualitatively reproduce the measured spectra. Such a large temperature differential is sufficient to substantially reduce (30%) the ion-acoustic frequency in comparison to its adiabatic value. Since no such shift was observed, it is safe to assume that the observed enhancements of the ion-acoustic resonance were not caused by a reduction in Landau damping due to unequal electron and ion temperatures.

In light of the scattering results from the composite Ar-He plasmas, it is clear that the presence of a heavy-ion impurity is capable of substantially affecting the ion-acoustic resonance frequency. Since copper and tungsten impurities are known to exist in the plasma used for this experiment, it is of interest to examine this possibility in more detail. If, for example, a 1% abundance of copper and tungsten was found in a helium plasma, the average atomic weight of the plasma would go from 4 to 6.4. This would shift the frequency of the ion-acoustic resonance by about 21%. In argon, such a shift for the same impurity concentration would only amount to about 2%. As a result, there should appear to be a difference of about 19% between the expected positions of the helium and argon resonances. Such a difference is not observed in the data; consequently, the impurity concentration of both copper and tungsten must be less than 1%, which, incidentally, is a more stringent limit than that imposed by the spectroscopic measurements.

From all of the theoretical models previously discussed, the BGK theory proved most successful in reproducing the data. Theoretical curves due to the BGK theory are presented alongside the data in Figs. 16 and 17. These

curves were calculated for the specific plasma temperatures and densities that were measured by independent diagnostics. No free parameters were used in the calculations other than a normalization of the calculated spectra to the peak amplitude of the data so as to allow for the uncertainty (factor of 2) in the absolute intensity calibration of the detection system. The BGK theory also predicts the enhancement of entropy fluctuations at zero frequency; however, this could not be verified in the present experiment because the finite pulse length of the laser and low-frequency variations of the laser absorption in the plasma imposed a lower limit on the detection frequency.

Even though the general shape and position of the ion-acoustic resonances is predicted fairly well by the BGK theory, there exists a discrepancy between the measured and predicted widths of the resonances. This difference, except for the 4.7 argon spectrum, cannot be accounted for by the finite resolution of the experiment ( $\Delta F=6$  Mhz,  $\Delta k/k=0.05$ ). A calculation where the finite wavelength and frequency resolution of the experiment are convoluted into the theory is also displayed alongside the data as a set of dashed curves. The basis for this discrepancy probably lies in the fact that ion-electron collisions have been assumed to be unimportant in the theoretical formalism. For plasma conditions encountered in this experiment, however, such an assumption is most likely invalid because the collisional equilibration time between electrons and ions [ $\nu_{ei}(\text{He})\approx 9$  nsec,  $\nu_{ei}(\text{Ar})\approx 70$  nsec] is comparable to the period of ion-acoustic oscillations. The main effect of collisional coupling between electrons and ions is to increase the effective thermal conductivity of the ions through contact with the highly conductive electrons. This increases the damping of ion-acoustic waves, thereby increasing the width of the observed resonances.

In the case of helium discharges, where the plasma may

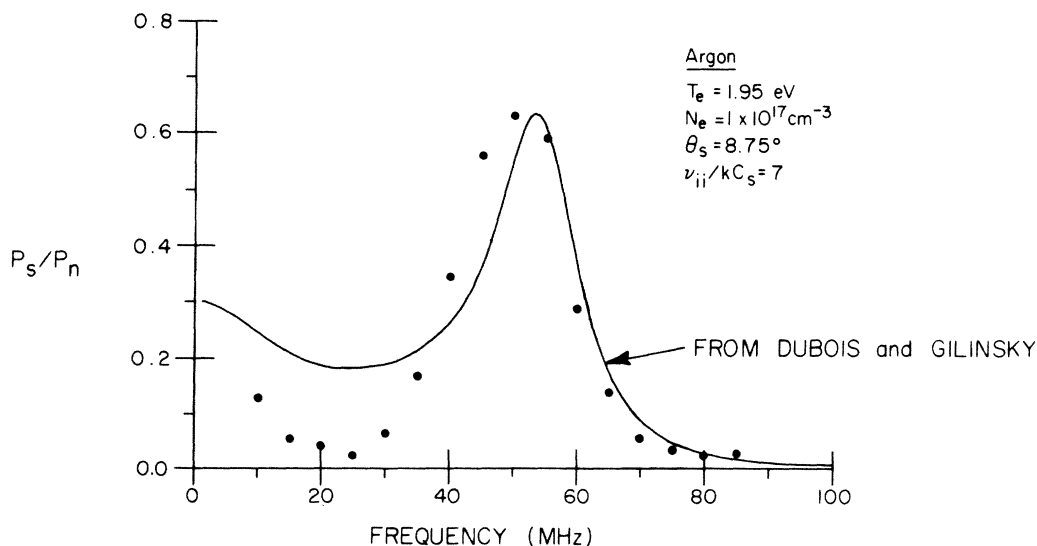


FIG. 20. Scattered light spectra in argon compared to theoretical predictions from the solution of the Balescu-Lenard equation (Refs. 3, 21, and 31).

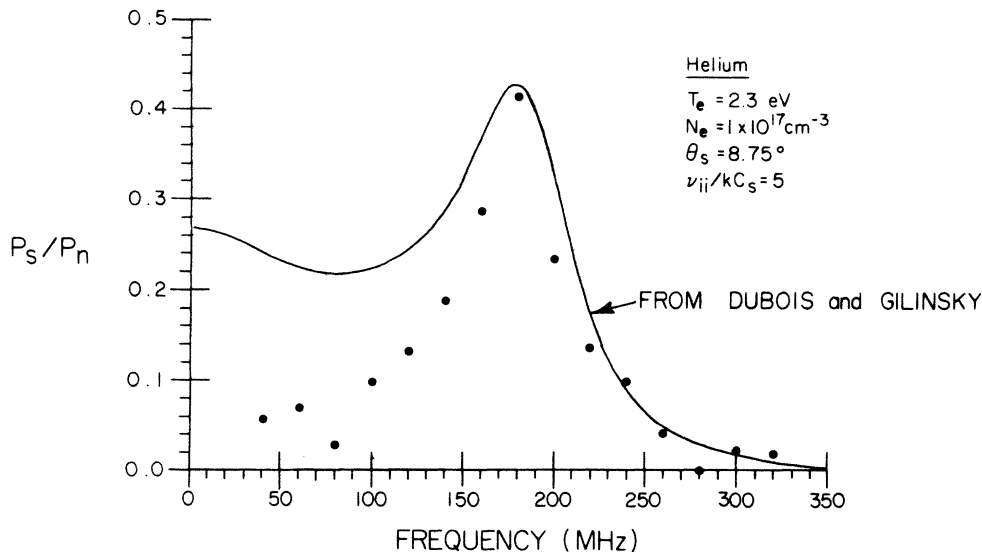


FIG. 21. Scattered light spectra in helium compared to theoretical predictions from the solution of the Balescu-Lenard equation (Refs. 3, 21, and 31).

not have been fully ionized, it is also possible that the ion-acoustic damping may have been increased by ion-neutral collisions. Of the various types of ion-neutral collisions, charge exchange collisions are the only ones with a sufficiently large cross section ( $\sim 10^{-14} \text{ cm}^{-2}$ ) to produce collision frequencies comparable to the ion-ion collision frequencies. These collisions could have produced damping by coupling the random motions of neutrals to the ordered motion of the ions. Nevertheless, even for comparable collision frequencies the damping due to charge exchange collisions is expected to be relatively minor because collisions of this sort transfer very little momentum in comparison to Coulomb collisions. Careful inspection of the data shows this to be true. In particular, a comparison of the  $8.75^\circ$  scattering data from the argon and helium discharges shows that the broadening of the ion-acoustic resonance with respect to the BGK predictions is about the same for both helium and argon. This is exactly what one expects to see if charge exchange collisions are not important since ion-acoustic spectra from argon plasmas, which were known to be fully ionized, could not have been broadened by charge exchange collisions.

Fluctuation spectra predicted by the Kivelson-Dubois solution of the Balescu-Lenard equation were also compared to the scattering data. These spectra are shown with data in Figs. 20 and 21 where, as before, the theoretical curves are normalized to the peak amplitude of the data. On the high-frequency side of the ion-acoustic resonance the theory produces a very good fit; however, at lower frequencies this model reproduces the data poorly. It appears that the approximations employed by Kivelson and Dubois, in solving the Balescu-Lenard equation, somehow overestimate the entropy fluctuation contribu-

tion to the total spectrum.

Finally, it is important to point out that the Fokker-Planck and Linnebur-Duderstadt models are in total disagreement with the data since they do not even predict the existence of an ion-acoustic resonance in highly collisional plasmas.

## VII. CONCLUSION

Small-angle scattering measurements of thermal ion-acoustic fluctuations from highly collisional ( $\nu_{ij}/kC_s \approx 5-13$ ) argon and helium plasmas have been obtained. These measurements show substantial enhancements of the ion-acoustic resonances due to collisional effects. A comparison to theoretical predictions calculated from independent measurements of temperature and density shows that the BGK theory is the most accurate in reproducing the data.

In addition to being very collisional, the plasma used in this experiment was characterized by a fairly large ( $g \approx 0.3$ ) plasma parameter. Thus, there was a good possibility that, with the exception of the Linnebur-Duderstadt model, the theoretical models examined in this work were inapplicable, due to their formal dependence on  $g$  being small. Nevertheless, even with  $g \approx 0.3$  the BGK and Balescu-Lenard models seem to be qualitatively correct.

## ACKNOWLEDGMENTS

It is a pleasure to acknowledge helpful discussions on the subject with H. R. Griem and the expert technical assistance of K. Diller. This work was supported by the National Science Foundation.

\*Present address: Naval Research Laboratory, Code 4730, Washington, D.C. 20375-5000.

<sup>1</sup>P. L. Bhatnagar, E. P. Gross, and M. Krook, *Phys. Rev.* **94**, 511 (1954).

<sup>2</sup>E. J. Linnebur and V. V. Duderstadt, *Phys. Fluids* **16**, 665 (1973).

<sup>3</sup>D. F. Dubois and V. Gilinsky, *Phys. Rev.* **133**, A1317 (1964), with corrections by N. B. McNelis and I. M. Tkachenko,

- Phys. Rev. A **21**, 1276 (1980).
- <sup>4</sup>M. S. Grewal, Phys. Rev. **134**, A86 (1964).
- <sup>5</sup>O. Theimer and M. M. Theimer, Nuovo Cimento Soc. Ital. Fisc. B **65**, 207 (1981).
- <sup>6</sup>E. M. Leonard and R. K. Osborn, Phys. Rev. A **8**, 2021 (1973).
- <sup>7</sup>E. Holzhauer, Phys. Lett. **62A**, 495 (1977).
- <sup>8</sup>A. A. Offenberger and R. D. Kerr, Phys. Lett. **37A**, 435 (1971).
- <sup>9</sup>J. H. Massig, Phys. Lett. **66A**, 2097 (1978).
- <sup>10</sup>A. W. DeSilva and G. Goldenbaum, *Methods of Experimental Physics* (Academic, New York, 1970), Vol. 19A, Chap. 3.
- <sup>11</sup>N. N. Bogoliubov, *Problems of a Dynamical Theory in Statistical Physics* (State Technical Press, Moscow, 1946).
- <sup>12</sup>Yu. L. Klimontovich, *The Statistical Theory of Nonequilibrium Processes in a Plasma* (MIT Press, Cambridge, Mass., 1967).
- <sup>13</sup>S. Ichimaru, *Basic Principles of Plasma Physics, A Statistical Approach* (Benjamin, New York, 1973).
- <sup>14</sup>E. E. Salpeter, Phys. Rev. **120**, 1528 (1960).
- <sup>15</sup>J. A. Fejer, Con. J. Phys. **38**, 1114 (1960).
- <sup>16</sup>M. N. Rosenbluth and N. Rostoker, Phys. Fluids **5**, 776 (1962).
- <sup>17</sup>J. P. Dougherty and D. T. Farley, Proc. R. Soc. London, Ser. A **259**, 79 (1960).
- <sup>18</sup>N. A. Krall and A. W. Trivelpiece, *Principles of Plasma Physics* (McGraw-Hill, New York, 1973) p. 389.
- <sup>19</sup>J. Sheffield, *Plasma Scattering of Electromagnetic Radiation* (Academic, New York, 1975).
- <sup>20</sup>R. Kubo, *Reports on Progress in Physics*, edited by A. C. Stickland (Institute of Physics and the Physical Society, London, 1966).
- <sup>21</sup>M. G. Kivelson and D. F. Dubois, Rand Corporation Report No. RM-3755-PR, 1963 (unpublished).
- <sup>22</sup>L. Onsager, Phys. Rev. **38**, 2265 (1931).
- <sup>23</sup>R. D. Mountain, Rev. Mod. Phys. **38**, 205 (1966).
- <sup>24</sup>R. K. Osborn, Phys. Fluids **11**, 595 (1968).
- <sup>25</sup>S. Chandrasekhar, Rev. Mod. Phys. **15**, 1 (1943).
- <sup>26</sup>R. Zwanzig, *Lectures in Theoretical Physics*, edited by W. E. Brittin, W. B. Downs, and J. Downs (Wiley, New York, 1961), Vol. 3.
- <sup>27</sup>H. Mori, Prog. Theor. Phys. **33**, 423 (1965).
- <sup>28</sup>R. Cauble (private communication).
- <sup>29</sup>R. Cauble and J. J. Duderstadt, Phys. Rev. A **23**, 3182 (1981).
- <sup>30</sup>H. R. Griem, *Plasma Spectroscopy* (McGraw-Hill, New York, 1964).
- <sup>31</sup>A. N. Mostovych, Ph.D. Thesis, University of Maryland, 1984 (unpublished).
- <sup>32</sup>R. E. Slusher and C. M. Surko, Phys. Fluids **23**, 472 (1980).
- <sup>33</sup>E. Holzhauer and J. H. Massig, Plasma Phys. **20**, 867 (1978).
- <sup>34</sup>R. J. Keyes and T. M. Quist, in *Semiconductors and Semimetals*, edited by R. K. Willardson and A. C. Beer (Academic, New York, 1970), Vol. 5.
- <sup>35</sup>H. Z. Cummins and H. L. Swinney, *Progress in Optics*, edited by E. Wolf (North-Holland, Amsterdam, 1970), Vol. 8.
- <sup>36</sup>G. Bekefi, *Radiation Processes in Plasmas* (Wiley, New York, 1966).